Optimal Energy Management Strategies and Mission Profiles for a generic Hybrid Aircraft

Oliviero, F.; Swannet, K.

Important note
To cite this publication, please use the final published version (if applicable).
Please check the document version above.

Optimal Energy Management Strategies and Mission Profiles for a generic Hybrid Aircraft

F. Oliviero[1] and K. Swannet.[2]
Delft University of Technology, Faculty of Aerospace Engineering, Delft, the Netherlands

The present paper shows the main characteristic of a numerical simulation tool, developed in the framework of the European H2020 project *MAHEPA*, to estimate optimal flight performance of a generic aircraft featuring a Hybrid powertrain. The purpose of the study is to determine optimal flight trajectories together with optimal power controls when a powertrain with multi-energy or multi-power sources (as the case of a generic hybrid one) is considered. For this purpose a complete new software has been developed, which is composed by three main parts: a mission performance "analyser" where the system dynamics of the problem is determined and it solves the aircraft Equation of Motion; a powertrain simulator that determines the operating conditions of the powertrain components and it ultimately computes the consumption of each energy source; a numerical algorithm that optimizes the aircraft control variables to determine both the optimum flight trajectory and the power management according to a certain objective functions and a variety of constraints. Different study cases are discussed when two existing flying hybrid aircraft are considered: a Hybrid-Electric (HE) *Pipistrel Panthera* aircraft and a Fuel-Cell hybrid (FCH) *Pipistrel HY4*. Results are presented also depending on the capability to simulate the entire mission as a whole (Single-Phase approach) as well as through the distinction of different flight segments as in the case of the Multi-Phase approach. In addition, two different resolution algorithms are tested in order to evaluate what are the aspects that might dictate the selection of the most suitable one.

I. Introduction

Predicting the flight performance of an aircraft is an essential analysis task to be performed during both design process and the execution of an actual operating mission. If possible, this is even more critical when looking at the performance of an aircraft equipped with a generic Hybrid Powertrain because of two main complementary reasons:

- The wrong depletion of energy/power during a certain mission can preclude the fulfilment of the mission. For instance, when considering an aircraft with a Hybrid Electric powertrain, if batteries are used in a wrong manner, it could be impossible to complete a demanding flight segment such as a climb or a pull up maneuver at the later stages of the mission.

- When low energy density sources are considered (such as again batteries), the identification of a proper nominal mission has dramatic impact on the overall design of the aircraft. For instance, when considering in the mission analysis a climb performed at a constant climb rate or with a linear variation of its value, the resulting MTOW might differ notably with consequences on the entire conceptual configuration of the aircraft.

The activities presented in this paper are therefore oriented in determining the flight performance together with the powertrain control parameters of a generic Hybrid, propelled powered aircraft; those studies have been developed in the framework of the H2020 European project *MAHEPA* (Ref. [1]), that aimed to design, manufacture and test in flight two different hybrid aircraft, as reported in Fig. 1; a Hybrid Electric (HE) *Pipistrel Panthera*, where an electric generator (coupled with a piston engine) and a battery pack are joined in a serial architecture; a Fuel Cell Hybrid (FCH) *Pipistrel HY4,* whose the powertrain consists of fuel cell, fed by an hydrogen tank, and a battery pack again in

---

[1] Lecturer/Researcher, Flight Performance and Propulsion, Kluyverweg 1, 2629HS Delft, f.oliviero@tudelft.nl
[2] MsC Student, Flight Performance and Propulsion, Kluyverweg 1, 2629HS Delft

a serial architecture fashion. These two platforms represent the reference study case for the present optimal performance study.

Fig. 1: the Hybrid Electric Pipistrel Panthera (left) and the Fuel Cell Hybrid Pipistrel HY4 (right)

During early conceptual design stages, the performance of a conventional propelled aircraft can be easily computed by looking at the point mass Equations of Motions; usually also different derivations of the Breguet formula are considered in order to determine fuel consumption along a certain mission, in presence of a variety of assumptions (e.g. cruise at constant speed and constant altitude, straight flight at constant power, etc…); an extensive literature exists on the topic (for instance Ref. [2], Ref. [3]) from which a complete set of equations can be extrapolated to determine a mathematical closed form of the problem. In addition, conditions that minimize the burnt fuel can be identified for each flight segment, (see for instance Ref. [4]).

From a mathematical point of view, the performance analysis of a Hybrid Aircraft poses multiple questions and it complicates its analysis because of several aspects, briefly discussed in the following bullets:

- By definition of Hybrid vehicle, it is possible to extract useful energy for motion from at least two different sources; therefore, an additional degree of freedom is necessary (or even more, depending on the number of energy sources and on the powertrain architecture) to fully describe the system dynamics; usually the additional variable is associated to a Power Management Control Device (PMCD) that regulates the power levels extrapolated from the different branches at each instant of the mission.

- All the classic performance analyses are based on certain known characteristics for either a propelled powertrain or a Turbofan/Turboprop one. With the introduction of new powertrain components, those assumptions can be no longer applied and therefore the classic solutions for the aircraft performance at different flight segments could not be valid for a Hybrid aircraft case. As an example, contrary to a Internal Combustion Engine (ICE), an Electric Motor doesn't suffer of altitude power lapses and its power curve (Torque vs RPM) can be easily adapted to the motion requirements. Hence, the performance of the aircraft during climb might differ notably due to the less and different sensitivity to the altitude and to the flight speed.

- Hybrid Powertrain relying on electric power, can enable innovative propulsion conditions such as the utilization of a propeller for energy recuperation since the same Electric Motor can be easily converted in an Electric Generator, with the possibility to re-charge an electric accumulator (i.e. battery pack). This recharging condition can in principle be done during certain flight segments where the power required for flight is low or even zero (i.e. descend). Again, during relatively low power conditions such as cruise, part of the energy source (for instance the thermal one) can be used to re charge the second one (the battery). Therefore, it is possible to identify several working modes for which the power flows vary drastically influencing the overall performance analysis and the optimal energy management.

In this contest, the present study proposes a method to determine optimal solutions for simultaneously the Power Management and Flight Trajectories parameters for an aircraft equipped with a generic Hybrid Powertrain.

From section II to section V, a brief overview of the methodology and the developed tool(s) is discussed whereas in section VII the preliminary optimal results are discussed for the selected study cases.

II.   Overall methodology

The conceptual approach adopted in this study is to couple the performance analysis of a generic Hybrid Aircraft to an optimal control resolution. This approach has been already applied in previous works related to performance estimation of Hybrid and Full Electric Aircraft (Ref.[5] and Ref.[6]). In this way, the present study turns into an optimization problem that aims at findings the optimal value for a proper set of control variables, capable to minimize a certain objective function, in presence of a certain set of constraints.

The optimization method, that is described in the section III, requires two additional analysis steps: first, a Mission Analysis that is capable to identify and solve the aircraft Equation of Motion, returning the required power for flight at each point of the mission. Secondly, a powertrain simulator is needed in such a way, energy depletion from the different sources can be updated during the entire flight; this calculation is therefore strictly depending on the operating characteristics of each powertrain component as well as on its overall architecture. Detailed information on the Mission Analysis and the Powertrain Simulator are reported in Section IV and V respectively.

All the three analyses steps have been implemented in a unique tool, named ITHACA (opt**I**mal **T**rajectory of **H**ybrid **A**ir**C**r**A**ft), whose the general functioning scheme is reported in Fig. 2, where it can be noted that the overall procedure requires an highly iterative approach.
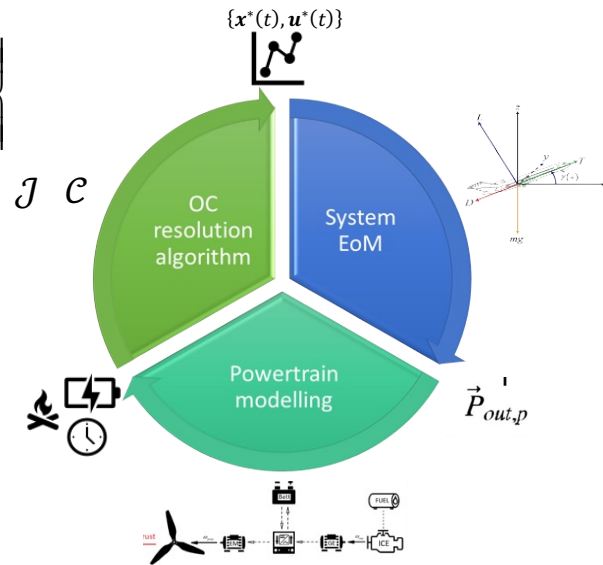
Fig. 2: Conceptual functioning scheme of the Hybrid Flight Performance Optimizer

III.   Optimal Control

An optimal control problem aims at finding the minimum (or maximum) of a certain functional index ($\mathcal{J}$) depending on a set of time dependent control parameters ($\boldsymbol{u}$), while obeying the system dynamics and boundary conditions through the state function ($\boldsymbol{x}$) and the path constrains ($\boldsymbol{c}$). A summary of the optimisation problem is given in the equation system below:

$$\begin{cases} Optimal\ Trajectory: & \{\boldsymbol{x}^*(t), \boldsymbol{u}^*(t)\} \\ System\ Dynamics: & \dot{\boldsymbol{x}} = \boldsymbol{f}(t, \boldsymbol{x}, \boldsymbol{u}) \\ Constraints: & \boldsymbol{c_{min}} < \boldsymbol{c}(t, \boldsymbol{x}, \boldsymbol{u}) < \boldsymbol{c_{max}} \\ Boundary\ Conditions: & \boldsymbol{b_{min}} < \boldsymbol{b}(t_0, \boldsymbol{x_0}, t_{fin}, \boldsymbol{x_{fin}}) < \boldsymbol{b_{max}} \\ Cost\ functional: & \mathcal{J} = \Phi(t_0, \boldsymbol{x_0}, t_{fin}, \boldsymbol{x_{fin}}) + \int_{t_0}^{t_{fin}} \boldsymbol{g}(t, \boldsymbol{x}, \boldsymbol{u})\, dt \end{cases} \quad (1)$$

3

The actual problem is continuous and thus infinite-dimensional. A wide literature exists properly dedicated to transcript and numerically resolve optimal control problems Ref. [7]. The authors in this case refer to existing algorithms based on the so called *Collocation Methods* Ref.[8] and already implemented in a *Matlab* open-source toolbox named *ICLOCS (*Ref.[9], [10], [11]); in this case, both the states variables $x(t)$ and the control variables $u(t)$ are single or multi-segment parametric functions (polynomial for instance) preliminarily prescribed by the user.

In collocation methods, the system dynamics is verified (either in a derivative or in an integral form) on a finite set of collocation points along the whole mission so that the differential equation reported in the system dynamics of the problem Eq.(1) can reduce to a set of algebraic equations. All the collocation methods consist in discretizing the time dependent solution and in approximating it by means of a certain functions basis; therefore it is important to distinguish the following points:

- *Collocation points* are points where the system dynamics (i.e. derivative or collocation constraints) defined in the problem (1) are evaluated.
- *Knot points* are points that are used to discretize the solution in different time interval. The solution in between two consecutives knot points is said *segment.*
- *Nodes* are points used to interpolate the solution function, meaning that its function approximation is exact on those points

The number and location of those points is different depending on the type of used algorithm. In the present study, two different collocation algorithms are tested; the *Hermite-Simpson Direct Collocation* (Ref. [12], Ref [13]) and the *Legendre-Gauss-Radau (LGR) Pseudospectral* (or *Global Orthogonal*) *Collocation Method* (Ref. [14]). The difference between HS and LGR discretization is shown in Fig. 3.
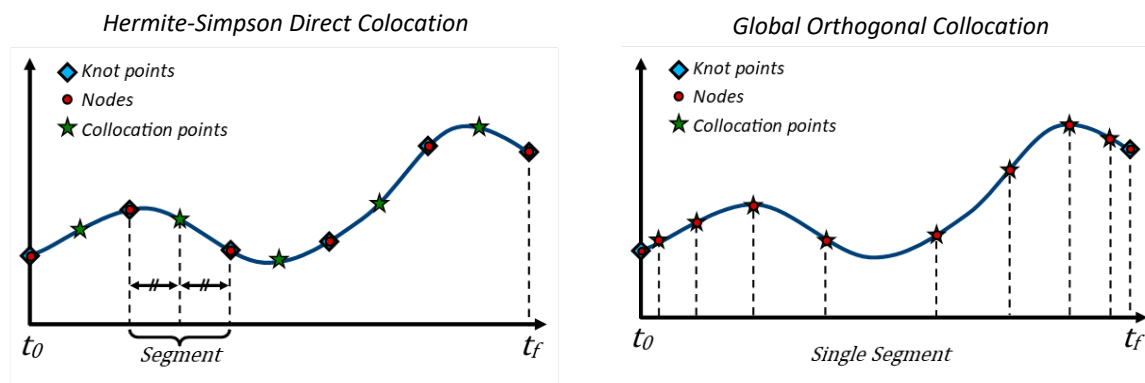
Fig. 3: Approximation approaches for HS Direct Collocation (left) and LGR Pseudospectral (right)

It can be seen that *Hermite-Simpson* is a local collocation method, and splits the time domain in equal-length segments, with the knot points used as nodes for interpolation and collocation points placed in the segment midpoints. Global *Legendre-Gauss-Radau* Pseudospectral, however, keeps the time domain as a single segment, and places both the nodes and collocation points in Gaussian quadrature points. It is possible to use multiple segments with LGR, called local orthogonal collocation. However, this is a less efficient method, as global orthogonal collocation achieves spectral accuracy. Specifically, the Radau form of Legendre-Gauss collocation will be used. This version of global orthogonal collocation does not collocate the final (knot) point, further increasing its convergence rate. Finally, Hermite-Simpson uses cubic Hermite polynomials to interpolate the solution, and Simpson quadrature to approximate integrals. Legendre-Gauss-Radau on the other hand uses piece-wise Lagrange polynomials for interpolation, and Legendre-Gaussian quadrature for integral approximation. Overall, this means global orthogonal collocation is the better method when the control function is sufficiently regular over the time domain.

It is worth to note that initial and final conditions need to be known and non-linear constraints ($c(t, x, u)$) can be applied to take particular trajectory or system dynamics conditions into account such as the avoid of stall during the entire flight.

The Problem (1) is related to the so-called Single Phase Optimal Control, where the entire flight trajectory is considered as a whole and therefore no intermediate (boundary) conditions can be included: hence, when applied to an aircraft trajectory optimization, those methods don't allow to distinguish intermediate flight segments as climb, cruise, descend, etc...

In order to specify different flight segments, a Multi-Phase approach is needed; in fact, a Multi-Phase allows to describe a dynamic system that presents different sets of (dynamic) algebraic equation or boundary conditions as it is the case of the different segments of a typical flight mission. It is worth to mention that, to solve Multi-Phase problems the sequence of the transition (e.g. take-off →climb→cruise→etc…) must be preliminarily known. Hence, to allow for Multi-Phase control, a set of boundary constrains are imposed to link each phase together and allow for continuous (in C0) state transition between phases as shown in Fig. 4.
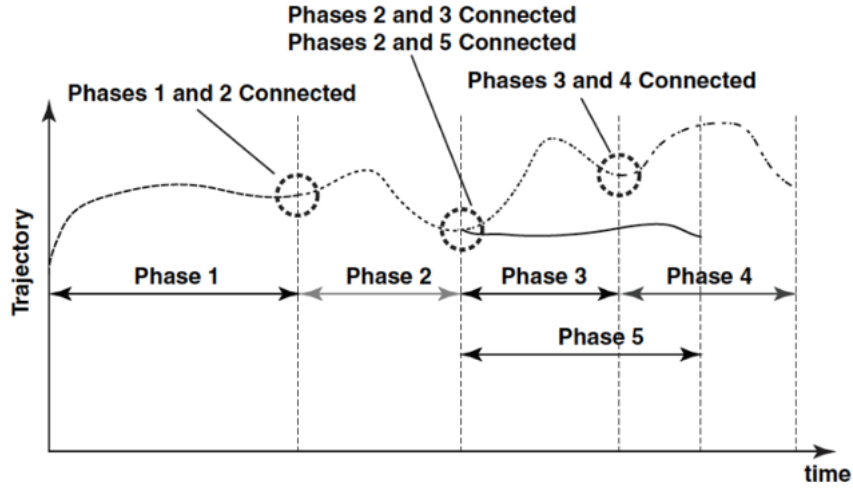
Fig. 4: Multi-Phase Optimal Control Problem, from Ref. [15]

In multi-phase problems, the total cost (or performance) index is the sum of the cost functional in each of the P phases:

$$\mathcal{J} = \sum_{p=1}^{P} \mathcal{J}_p \quad p = 1,2,\dots,P \tag{2}$$

The linkage constraint $\mathcal{L}^p$ at a given phase boundary $\boldsymbol{p}$ takes the form given by the following equation:

$$\mathcal{L}^p\left(x^{(p-1)}, t_f^{(p-1)}, \quad x^{(p)}, t^{(p-1)}, \quad \right) = 0 \tag{3}$$

The link constraint generally expressed in the form of Equation (3), ensures the continuity of the states across the different phases of the control problem and therefore an appropriate set of equations must be applied at each phase's link, additionally to the set of trajectory and system constraints.

IV. Aircraft Dynamics

In order to assess the aircraft performance along a certain mission, the aircraft is first reduced to a point mass model and therefore the trim is not considered. Additionally, only motion of the aircraft in its longitudinal plane is considered, so no lateral forces, yaw and roll motions are considered. Neglecting also the presence of possible wind, the motion of the aircraft can be represented by the following system of equations in relation to the angles and vectors defined in Fig. 5:

5

$$\begin{cases} \dot{d} = V \cos(\gamma) \\ \dot{V} = \frac{T-D}{m} - g \sin(\gamma) \\ \dot{h} = \dot{z} = V \sin(\gamma) \\ \dot{\gamma} = \frac{L}{mV} - \frac{g \cos(\gamma)}{V} \end{cases} \tag{4}$$

The system of equations (4) can be further specialized for each of the flight segments that will correspond to the "phase" of a Multi-Phase control problem; to do that, proper boundary conditions need also to be specified especially at the initial and final status of each segment for either the control and/or the state variables. In order to solve those equation of motion, only top-level information of the aircraft is necessary. In this specific case, only the Drag Polar of the aircraft and its Lift Curve (Lift Coefficient vs Angle of Attack) are needed. When also Take-Off and other low speed segments are included, that aerodynamic information can be further specialized and further Phases can be included in the initialization of the optimization problem (e.g. introducing different Drag Polars that account for the deployment of High Lift Devices).
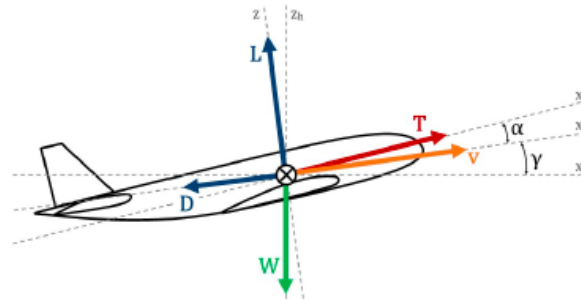
Fig. 5: Aircraft reference coordinate systems

V. Powertrain Simulator

A simulator tool has been developed in house following an Object-Oriented approach. The main purpose of this strategy is to generalize a wide variety of powertrain architectures that in principle can be included by the identification of its components and their linkage. Fig. 6 displays the Hybrid Electric Power System Class developed to instantiate different powertrain architectures. This class can be composed of an arbitrary number of component subclasses such as Batteries, Fuel Cells, Engines and Propellers. Each component class contains properties and method specific to each class topology; those methods are used to derive component performance. In order to instantiate a powertrain, the user has to determine the type of architecture (series or parallel), and the connections of the components. For each one of the selected components, the performance can be modeled either through an analytical model or a data map derived from experimental measurements; this can be specified in each instantiation of each powertrain component object.

The modularity of the code is achieved by applying the *SOLID* principles for object-oriented programming which also ensure the code is sustainable. The SOLID principles can be resumed in the following:
- *Single-Responsibility Principle*: Each piece of code (class, method, or function) should have only a singleresponsibility or purpose.
- *Open-Closed Principle*: Each piece of code should be open to for extension, but closed to modification, meaning existing code should not require modification when functionality is added.
- *Liskov Substitution Principle*: If functions are redefined in subclasses, their behavior must remain the same to that of the function in the base class, e.g. same input and output types.

6
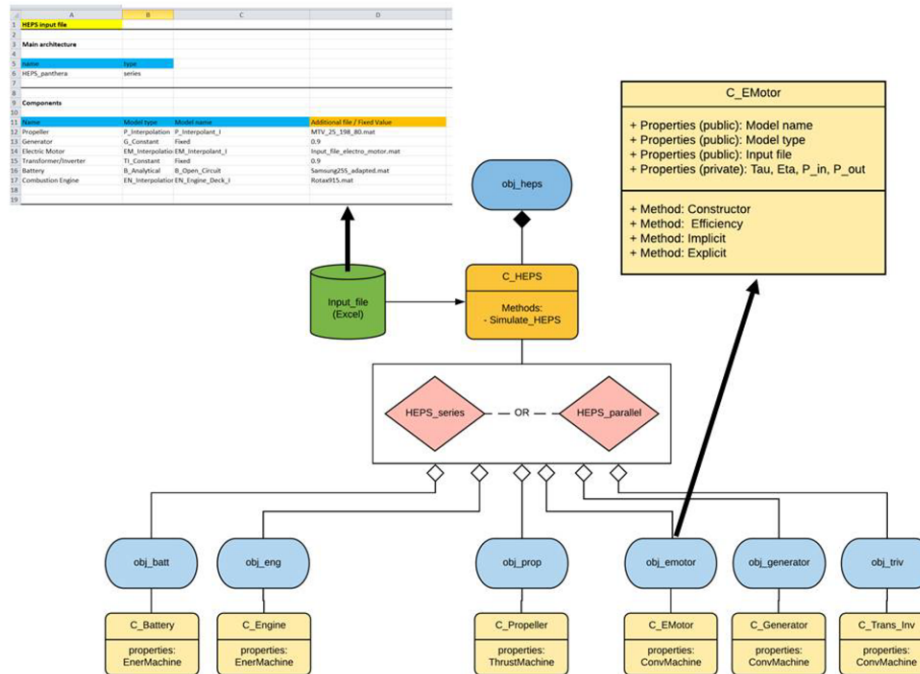
Fig. 6: Identification and simulation of the powertrain components by means of the OO paradigm

- *Interface Segregation Principle*: Subclasses should not inherit methods they do not require. Therefore, methods should be separated from certain classes if required.
- *Dependency inversion Principle*: Classes should not depend on specific subclasses, but on abstractions.

As a result, the two different powertrains of both the *Pipistrel Panthera* and the *Pipistrel HY4* have been simulated by using the same tool. As it can been seen in Fig. 7, although they present the same serial architecture with the same E-motor , all the remaining components are case specific and they have been modeled by using different instantiations of the OO classes shown in Fig. 6.
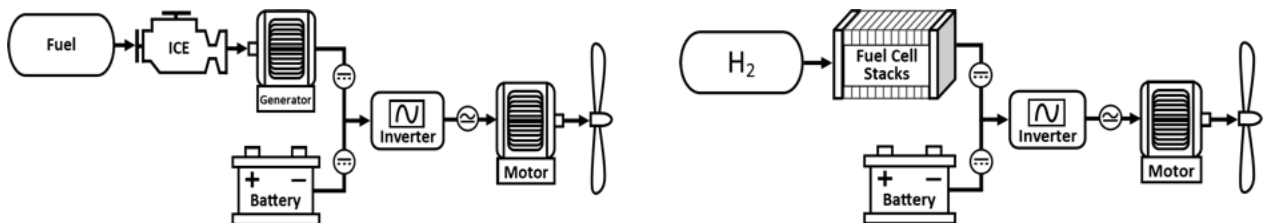
Fig. 7: Powertrain sketches of the Pipistrel Panthera (left) and of the Pipistrel HY4 (right)

Both analytical relations and look up tables can be used to model the operating characteristics of the powertrain components. In the present study, semi-empiric analytical relations are used to model the efficiency of the fuel cell and the battery so that both hydrogen consumptions and battery State of Charge can be calculated at each instant of the mission.

7

A. Proton-Exchange Membrane Fuel Cell

The proton-exchange membrane fuel cell, also called the solid polymer fuel cell, is the considered fuel cell type used in the *Pipistrel HY4*. A solid-polymer ion-exchange-membrane serves as the electrolyte. Performance is approximated using the static, semi-empirical model presented by Ref. [16], where, for a given current draw, the cell voltage is found by first determining the open-circuit voltage (V_{OC}), which is the voltage when no current flows, and subtracting the activation (V_{act}), ohmic (V_{ohm}), and concentration (V_{conc}) voltage losses or over-potentials:

$$V_{FC} = V_{OC} - V_{act} - V_{conc} - V_{ohm} \tag{5}$$

The open-circuit voltage is determined using Nernst equation to correct the ideal voltage for non-standard temperature and pressure as shown in Eq. (6), where R is the universal gas constant, F is Faraday's constant, $n_{ean} = 2$ is the number of electrons involved in the anode reaction and p_{H2} and p_{O2} are the partial pressures of hydrogen and oxygen gas in atmosphere respectively.

$$V_{OC} = V_0 - 0.85 \cdot 10^{-3} (T_{oper} - 298.15) + \frac{RT_{oper}}{n_{ean}F} \ln \left(P_{H2} \sqrt{P_{O2}} \right) \tag{6}$$

The activation over-potential is a non-useful voltage required to overcome the initial energy barrier and get the reaction going. The associated voltage loss is determined using the Buttler-Volmer equation (7), where α is the charge transfer coefficient, i_0 is the exchange current density, and n_e is the amount of electrons involved in the reaction. From Fuel cell reaction equations those values have a value of 2 and 4 for the anode and cathode respectively.

$$V_{act} = \frac{RT_{oper}}{F\alpha} \left(\frac{1}{n_e} \ln \left(\frac{i}{i_0} \right)_{catode} + \frac{1}{n_e} \ln \left(\frac{i}{i_0} \right)_{anode} \right) \tag{7}$$

Ohmic voltage losses are caused by resistance of the electrolyte membrane to the flow of ions, approximated by Ohm's law, Eq. (8), where membrane resistance, Rm, is assumed to be a constant value.

$$V_{ohm} = i\,R_m \tag{8}$$

Finally, concentration losses caused by reduced availability of reactants at high current densities are accounted by means of Eq (9) where i_{lim} is the maximum current density which can be achieved before electrodes are flooded with product water and the concentration of reactant gasses becomes so low that the reaction stops.

$$V_{conc} = \frac{RT_{oper}}{F} \left(\frac{1}{n_e} \ln \left(\frac{i_{lim}}{i_{lim}-i} \right)_{anode} + \frac{1}{n_e} \ln \left(\frac{i_{lim}}{i_{lim}-i} \right)_{cathode} \right) \tag{9}$$

When all the losses are considered, the stack power can then be found using Eq. (10), and Eq. (11) is used to obtain the hydrogen consumption. The electrical efficiency of the cell is found by taking the ratio of the cell voltage over the ideal voltage, as shown in Eq. (12).

$$P_{stack} = V_{FC}\, i\, A\, n_{cells} \tag{10}$$

$$\dot{m}_{H2} = \Lambda_{H2}\, M_{H2}\, \frac{I}{n_{ean}F}\, n_{cells} \tag{11}$$

$$\eta_{FC\,fuel} = \frac{V_{FC}}{1.229} \tag{12}$$

Fig. 8A shows the polarization curve obtained after running a parameter estimation using flight test data as reference data to determine the charge transfer coefficients, membrane area and resistance, exchange current density, and limit current density. While test bench data is available, and also shown, the flight test data is used for the parameter estimation instead, as it provides a more realistic idea of what performance to expect of the fuel cells during flight. The entire fuel cell performance model is therefore reported in Fig. 8B in terms of delivered power.
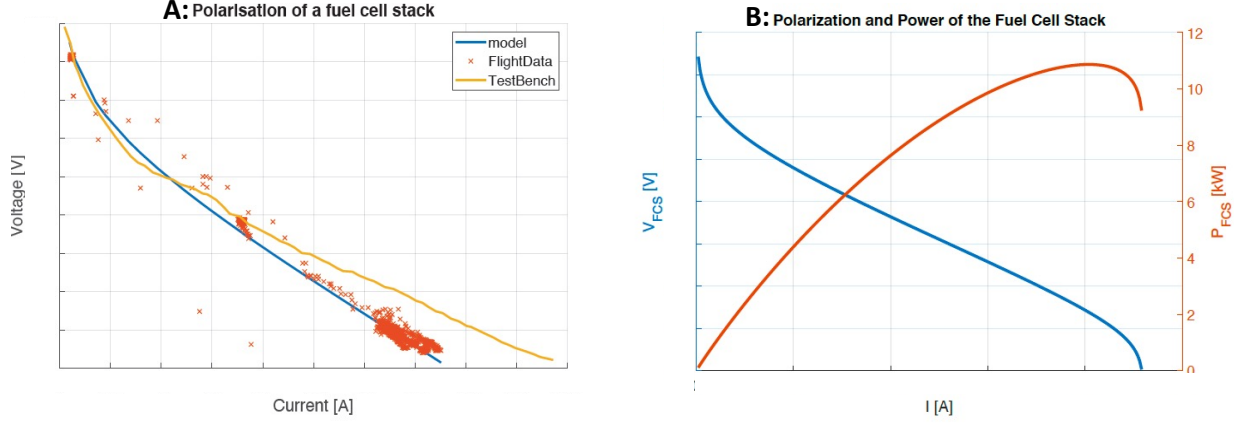
Fig. 8: polarization model (A, left) and power curve (B, right) of the selected fuel cell (values of Voltage and Current omitted due to proprietary information)

B. Lithium-Ion Batteries

Similarly, to the Fuel Cell, the batteries are modeled by means of an equivalent-circuit model based on the Rint model (Ref. [17]), for which the cell terminal voltage is determined by means of Eq. (13).

$$V_{cell} = V_{OC} - I_{cell}R_{cell} \tag{13}$$

First, the open-circuit voltage, V_{OC}, is determined using Eq. (14), which accounts for activation (logarithmic), ohmic (linear), and concentration (exponential) voltage losses as a function of the cell depth-of-discharge, DoD, being defined as the opposite of the State of Charge, SoC, and describes the relative amount of energy extracted from the battery, while SoC is the relative amount of energy which remains, meaning $DoD = 1 - SoC$. The maximum cell voltage depends on the cell technology and for lithium-ion cells is $V_{max}=4.2[V]$.

$$V_{OC} = V_{max} - K_1 \ln(K_2 \cdot DoD) - K_3 \cdot DoD - K_4 e^{K_5(DoD-K_6)} \tag{14}$$

Internal losses due to current draw are accounted for by the internal resistance value found using Eq. (15) where Q_{nom} is the nominal capacity of the cell being a parameter given by cell manufacturer. Eventually the discharge efficiency can be obtained from the ratio between the terminal cell voltage and the ideal open circuit voltage as in Eq.(16).

$$R_{cell} = \frac{K_7 e^{K_8 SoC} + K_9}{Q_{nom}} \tag{15}$$

$$\eta_{batt} = \frac{V_{cell}}{V_{OC}} \tag{16}$$

The empirical coefficients $K1$ through $K9$ are determined once again using parameter estimation when considering real discharging curves provided by manufacturer or by experimental measurements; resulting discharge curves are provided in Fig. 9 for both the HY4 and the Panthera battery packs. It is noted that the cells used in the Panthera are approximated with a root-mean-square percentage error of $\epsilon RMS = 0.79\%$ when compared to the actual discharge curves.
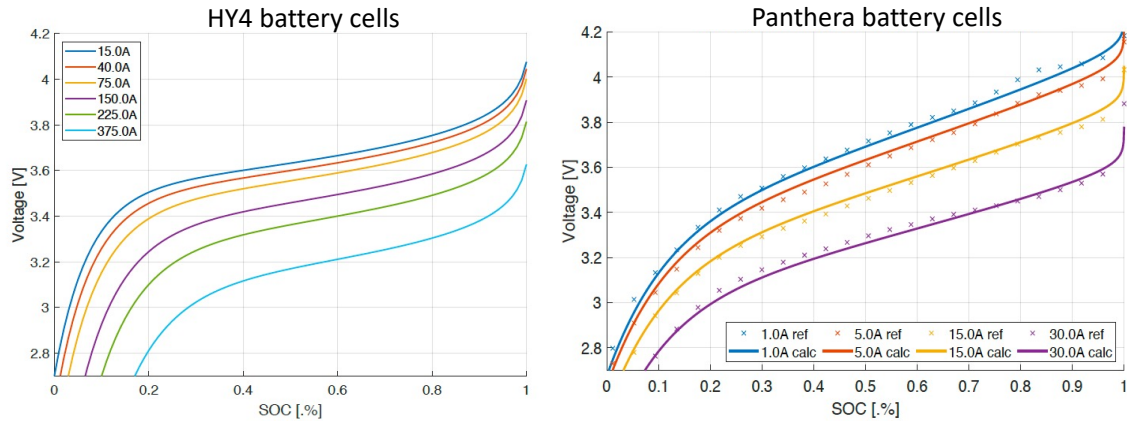
Fig. 9: Discharge curves for selected batteries of the Pipistrel HY4 (left) and Pipistrel Panthera (right)

C. Other powertrain components

With reference to the schemes of Fig. 7, the other components considered in the powertrain simulator are: Electric Motor, Electric Generator, Inverters/Converters, Gear Boxes, Internal Combustion Engine and Propeller (either fixed pitch or variable one). Those components are modeled by means of look up tables, extrapolated by either experimental measurements or manufacturer data. These maps link the electric (mechanical) input power to the electric (mechanical) output power, taking into account a certain efficiency depending on the operating condition. As an example, the efficiency map η of the considered electric motor is plotted in Fig. 10 against the rotational speed Ω and the torque τ at the propeller shaft (no gear box is considered).
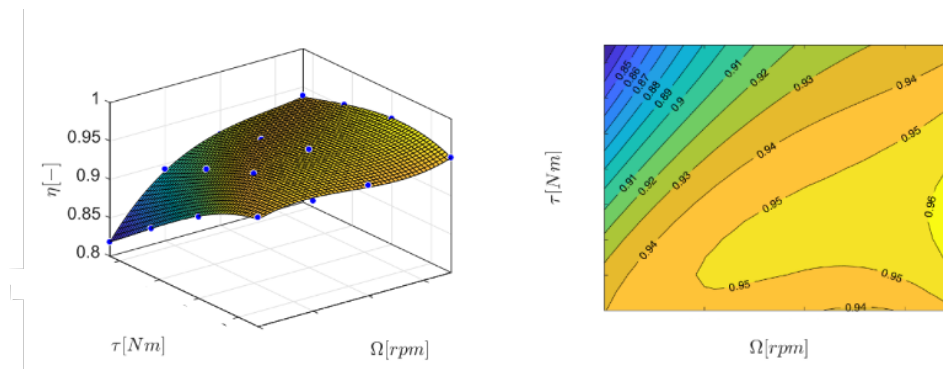
Fig. 10: efficiency map of the electric motor (values of Torque and Rotational Speed omitted due to proprietary information)

Considering the powertrain architecture defined by means of the OO class diagram defined in Fig. 6, the overall efficiency is calculated by simply multiplying accordingly all the contributions of the components; since the fuel cell or engine are controlled explicitly, as it is explained in Section VIII, the power drawn from the batteries is determined implicitly by linking all components together. First, Eq.(17) yields to the total electric power required at the E-Motor. Then, the battery power draw is found using Eq.(18) depending on the FC *HY4* or the HE *Panthera*. It is explicitly noted that in theory the battery power is allowed to assume negative values: in this case the system is recharging the battery from the main power branch (Fuel Cell or Electric Generator) if the flight segment allows for that.

$$P_{e\ in_{Emot}} = P_{shaft} \cdot \eta_{EM} \cdot \eta_{INV} \tag{17}$$

10

$$P_{batt} = \begin{cases} = P_{e\ in_{Emot}} - P_{FC} & (HY4) \\ \\ = P_{e\ in_{Emot}} - \eta_{GEN}P_{ICE} & (Panthera) \end{cases} \qquad (18)$$

VI. Validation

The purpose of the validation activities is to evaluate the reliability of the powertrain simulator model coupled to the aircraft dynamics as no optimal trajectories study have been found in literature to be replicated. In this contest, real flight data of the Pipistrel HY4 experimental test campaign (Ref. [18]) conducted in the framework of the MAHEPA project, (WP7: flight tests), are taken into account; in particular a 2-hours long flight, occurred on November 2020 at the Maribor airport (Slovenia) has been considered, whose the qualitative flight trajectory is shown in Fig. 11.
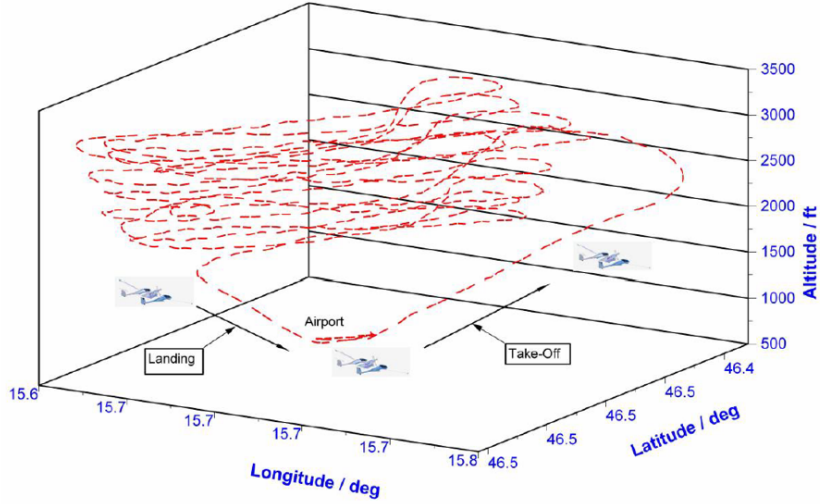
Fig. 11: flown trajectory of the HY4 on November 2020.

Considering the problem specification reported in the following section VII- A, the system dynamics of Eq. (23) is used to link the state variables and the control variables. The control variables u_t are read directly from the flight test data and used to reconstruct the state variable x_t, assuming that it varies linearly according to Eq. (19), with a time step $\Delta t=1$ s.

$$x_{t+\Delta t} = x_t + \dot{x}(u_t) \qquad (19)$$

No values are available for the flight path angle or its derivative, so the flight path angle is estimated by Eq. (20) using speed and altitude data instead;

$$\gamma_t = sin^{-1}\frac{h_{t-1}-h_t}{v} \qquad (20)$$

The comparison between reconstructed state variables and flown states is therefore reported in Fig. 12 for each state and also the Root Mean Square Error (RMSE) between reconstructed and recorded data is calculated; the results for the distance, altitude, and fuel mass have errors with an order of magnitude 10^{-2} whereas the indicated airspeed and battery state-of-charge show significant deviations. Investigating the origin of these errors leaded to the pitot-static system that had calibration issues and these errors are likely aggravated by the estimation of the flight path angle according to Eq. (20).

11
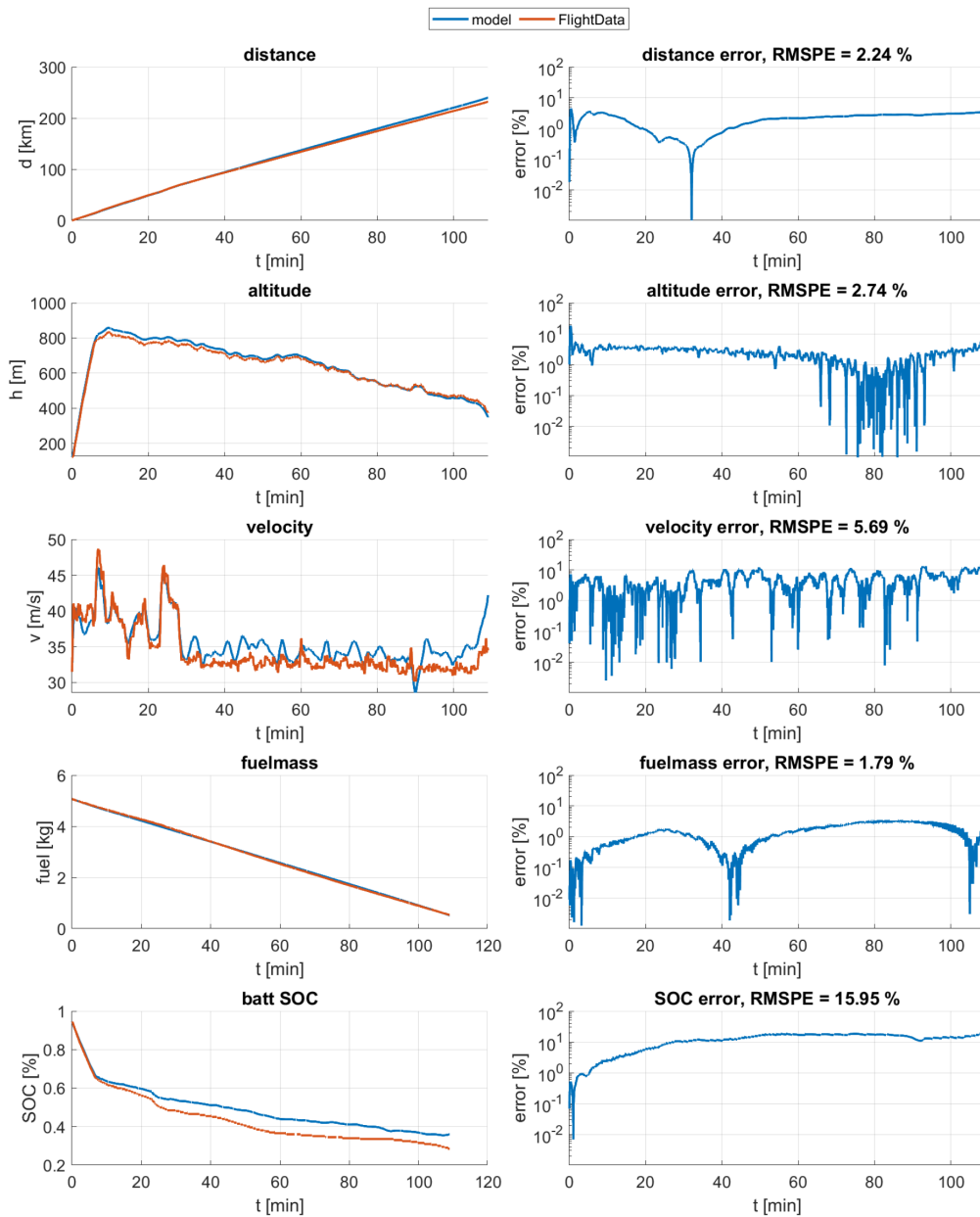
Fig. 12: HY4 state variables comparison

A comparison between the reconstructed shaft power and the recoded one is reported in Fig. 13 where again the effects of the with noise in the acquisition of the flight speed are visible and they return a RMSE=15%. In order to evaluate the possible impact, a second validation exercise is conducted, considering directly the power registered during the flight as input to reconstruct the powertrain behavior. Results are reported in this case in Fig. 14 only in terms of battery SOC. In this case, graph clearly shows that errors in the SOC computation are well below 5% so that models is considered to be suitable for mission analysis and the previous errors have been accounted to noise in signal acquisition during the flight.
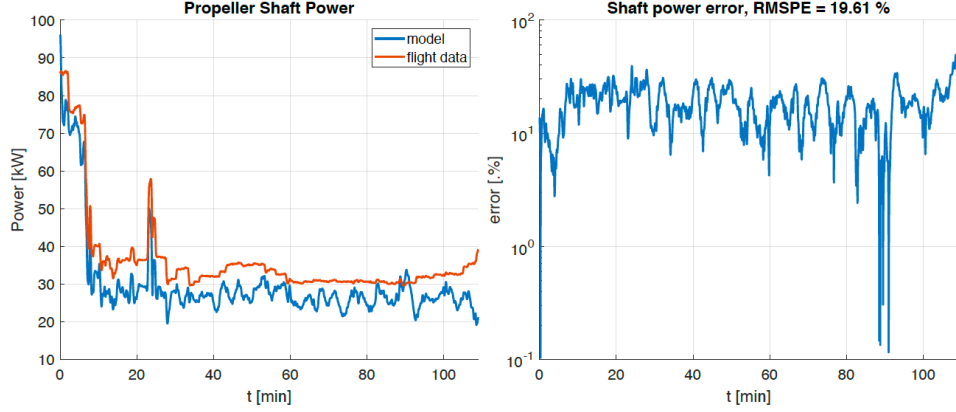
Fig. 13: propeller shaft power comparison
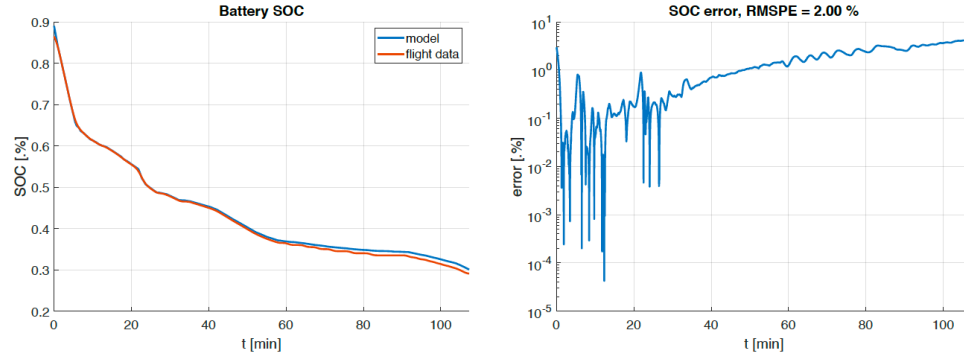
Fig. 14:updated battery SOC validation

VII.   Preliminary results

A. Definition of the study case

In the proposed optimal control problem, the states and controls variables are described by the two arrays variables $\boldsymbol{x}$ and $\boldsymbol{u}$ respectively.

$$\boldsymbol{x} = [d \quad h \quad v_{IAS} \quad \gamma \quad m_{fuel} \quad SOC] \tag{21}$$

$$\boldsymbol{u} = [P_{shaft} \quad \dot{\gamma} \quad \Omega_{prop} \quad \mathcal{U}_{CPS}] \tag{22}$$

The control variables array is composed by one variable related to the aircraft attitude (i.e. the derivative of the flight path angle) and three variables connected to the powertrain status: the Propeller shaft Power P_{shaft}, the Rotational Speed of the propeller Ω_{prop}, and a control parameter related to the main power branch $\mathcal{U}_{CPS}$; usage of the general parameter $\mathcal{U}_{CPS}$ and generalized equation for fuel mass rate, allows different powertrain configurations to be used without the need to alter the code, in accordance with the SOLID principles, discussed in section V; it can be specified as the normalized value of the fuel cell current drawn in case of the HY4 study case, or the Rotational Speed of the Internal Combustion Engine shaft for the Panthera study case.

The control and the state variables are connected thought the system dynamics specified in the system of Eq. (23):

13

$$\dot{x} = \begin{bmatrix} \dot{d} \\ \dot{h} \\ \dot{v}_{TAS} \\ \dot{\gamma} \\ \dot{m}_{fuel} \\ S\dot{O}C \end{bmatrix} = \begin{bmatrix} v_{TAS} \cdot \cos\gamma \\ v_{TAS} \cdot \sin\gamma \\ \frac{T-D}{m} - g \cdot \sin\gamma \\ \dot{\gamma} \\ f_{CPSfuel}(\mathcal{U}_{CPS}) \\ \frac{I_{batt}}{3600\, Q_{batt}} \end{bmatrix} \tag{23}$$

The indicated airspeed is used in the state vector, while the equations of motion, require the use of true airspeed. While adding an extra conversion step when determining the dynamics, using indicated airspeed as a state variable over true airspeed makes it easier to apply bounds. The indicated airspeed, assumed equal to calibrated airspeed and equivalent airspeed, does not vary with altitude, meaning any published airspeed limits can be applied as constant bounds.

In order to investigate the capability of the tool, two main objective functions are evaluated for each aircraft study case. The first on is related to the minimization of the fuel along a given range $d(t_f)$ as defined in Eq.(24); the fuel cost $\mathcal{J}_{fuel}$ is defined as the square of the percentage fuel used per 100km. This cost function was chosen as it normalizes the cost with respect to the range and the fuel capacity of the aircraft. The objective contains a second term that is the integral of the square of the flight path angle rate; it is introduced to avoid over-control of the flight path angle.

$$\mathcal{J}_{fuel} = \left[\frac{\left(1 - \frac{m_{fuel}(t_0)}{m_{fuel}(t_f)}\right) x 100}{d(t_f) x 10^5} \right]^2 + \int_{t_0}^{t_f} c_\gamma \cdot \dot{\gamma}^2(t) dt \tag{24}$$

A similar problem related to the minimization of fuel, is represented by the determination of maximum range, for which the considered functional is reported in Eq. (25). In this case the problem is the dual of Eq. (25), being the amount of consumed fuel and energy, known a priori.

$$\mathcal{J}_{range} = \left(d(t_f) x 10^5 \right)^2 + \int_{t_0}^{t_f} c_\gamma \cdot \dot{\gamma}^2(t) dt \tag{25}$$

Finally a second optimization problem, related to the minimization of the flight time over a certain range is used also as a term of comparison against the minimum fuel problem of Eq.(24); in this case the flight time is normalized with respect to the flight time required to fly the specified range at the maximum allowed airspeed, v_{NE}, that is known for both the considered aircraft:

$$\mathcal{J}_{time} = \left(\frac{t_f \cdot v_{NE}}{d(t_f)} \right)^2 + \int_{t_0}^{t_f} c_\gamma \cdot \dot{\gamma}^2(t) dt \tag{26}$$

The optimal control problems require the definition of proper bounds for both state and control variables as well as the determination of some path constraints that are applied at every point in time. In particular the system of Eq. (27), is applied in such a way battery, electric motor and propeller are always operating within the nominal conditions identified for each component:

$$g_{path} = \begin{bmatrix} I_{batt} \le I_{batt\,max} \\ \tau_{EM} \le \tau_{EM\,max} \\ J_{min} \le J \le J_{max} \end{bmatrix} \tag{27}$$

14

B. Results – HE Pipistrel Panthera

The flight profile, described by the altitude and airspeed, power setting, given by shaft power and propeller RPM, and energy management, defined by the engine RPM and (slope of) the battery state of charge, are plotted as a function of time in Fig. 15 for a variety of input ranges. The flight times are given in the figure legend. Additionally, these plots also include the results for the maximum range optimization, as conditions for fuel minimization and maximum range are the same.
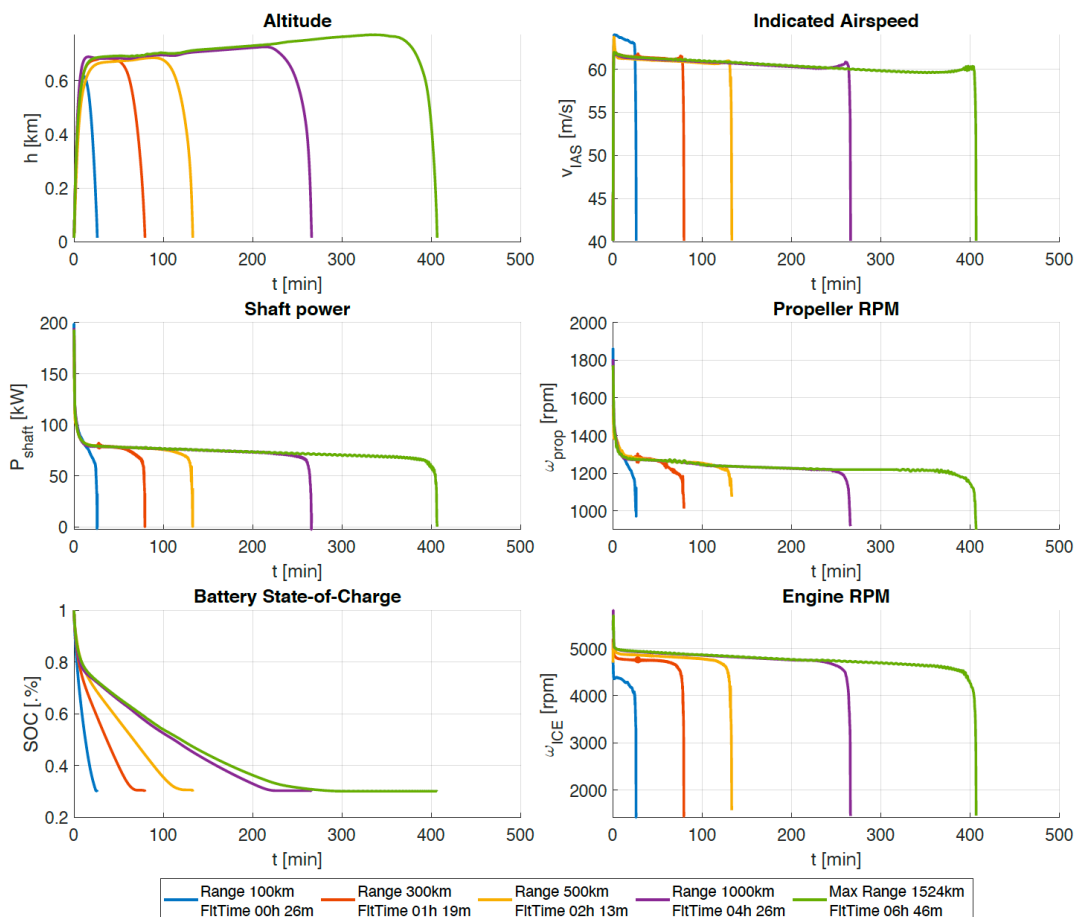
Fig. 15: Optimal flight trajectories for minimum fuel consumption, HE Pipistrel Panthera

The results show flight profiles which remain consistent at increasing the flown range. For shorter ranges where the cruise altitude is not reached before the start of the descent, the flight profile takes a parabolic shape. Additionally, the airspeed plot for a range of 100 km in Fig. 15 reaches a slightly higher value than the flight profiles for longer ranges. This is due to the batteries delivering relatively more power compared to longer range flights, as indicated by the steeper slope of the state-of-charge function. In addition, the Panthera has best fuel economy when flown at an altitude of h=700m at an indicated airspeed that matches also the analytical solution for the best range airspeed for propelled aircraft when including aerodynamic data of the Panthera. The batteries are used to boost power delivery during climb, after which the current drawn is reduced to a minimum, while still ensuring batteries are depleted at the end of the flight.

To evaluate differences with different flight trajectories, the results for minimum flight time, accounting for the same set of input range, are reported in Fig. 16. When minimum time is achieved, the Internal Combustion Engine runs continuously at its maximum power, while the batteries are fully depleted during the climb. The altitude at the top of the climb increases with range, and the maximum altitudes reached are now much higher than for the fuel-optimal flights. As a long climb requires the batteries to last longer, the discharge rate and airspeed are lower with increasing altitude and range. Once at the top of the climb, a descent is initiated to pick up airspeed.
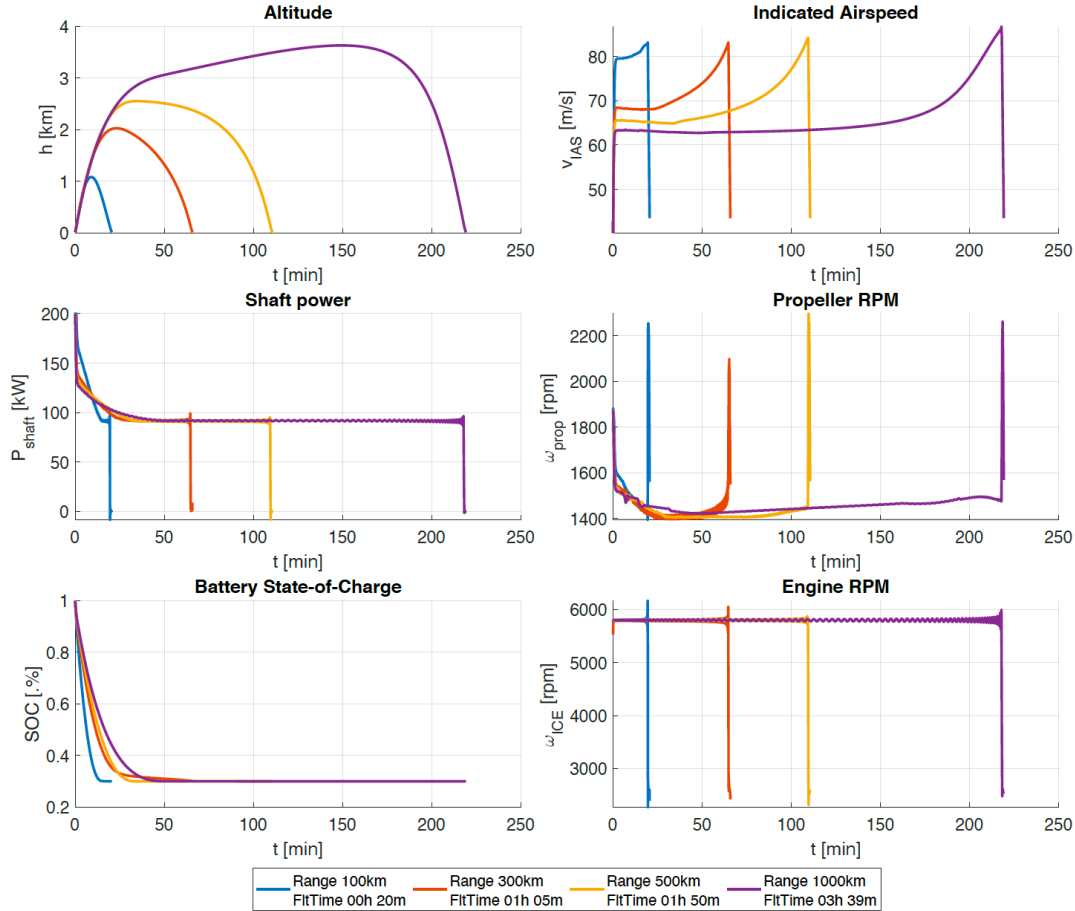
Fig. 16: Optimal flight trajectories for minimum time, HE Pipistrel Panthera

The flight times and differences in flight time and fuel consumption are listed in Table 1. Again, branding the 100 km case as an outlier, taking the weighted averages of the relative differences shows that the time-optimal trajectory reduces flight time by 17.6%, at a cost of 9.7% more fuel burn. For shorter ranges, the amount of power drawn from the batteries is higher, hence the fuel savings when flying a fuel-optimal trajectory increase rapidly with decreasing range. On the other hand, if time is the priority, this extra power from the batteries can be used to increase airspeed. For a range of 100 km, this means that the flight time can be reduced by 23%, but 26.1% more fuel will be burned compared to the fuel-optimal trajectory.

Table 1: Comparison of global results for minimum time and minimum fuel, HE Pipistrel Panthera

Range	Flight time (Min.)	ΔFlight time [h:mm]	Comparison with fuel-optimal case		
			ΔFlight time [%]	Δ Fuel burn [kg]	Δ% Fuel burn [%]
100	0:20	0:06	-23.1%	+2.3	+26.1%
300	1:05	0:14	-17.7%	+3.9	+11.9%
500	1:50	0:23	-17.3%	+5.6	+9.9%
1000	3:39	0:47	-17.7%	+10.2	+9.0%

16

C. Results -FCH Pipistrel HY4

Obtaining fuel-optimal trajectory solutions for the HY4 is significantly more challenging compared to the Panthera. The main reason for this seems to be the fact that the HY4 is relatively under-powered since its maximum Power-to-Weight ratio is nearly half of the Pipistrel Panthera meanwhile the Power-to-Weight ratio of the Fuel Cell System is about 30% of the one of the Electric Generator system (ICE+Generator) in the Pipistrel Panthera. This caused the optimizer to return trajectories where the altitude remains zero, presumable to avoid any scenario where power demand is high, like during a climb. To solve this, and force a climb, an additional integral cost function is added which equals one at every point where the altitude equals zero whereas it decreases quadratically as altitude increases until the cost becomes zero for altitudes equal to or higher than 300m. Results for this case are reported in Fig. 17; the general behavior of the functions is not far off from the ones obtained for the Panthera. It can be seen that the current drawn from the fuel cell is approximately constant throughout each of the flights, and changes in shaft power are entirely compensated by the batteries. The shaft power is consistent across the different ranges. Since the contribution of the battery to the total power is less for longer ranges, the fuel cell load is increased to compensate. The higher current draw from the fuel cells, however, is not sufficient to maintain the same airspeed, and both airspeed and propeller rpm are reduced as flight range increases. To complete the overview, a maximum range $d_{max}=620\ km$ can be achieved when consuming all the amount of hydrogen (equal to 14 kg) stored on board.
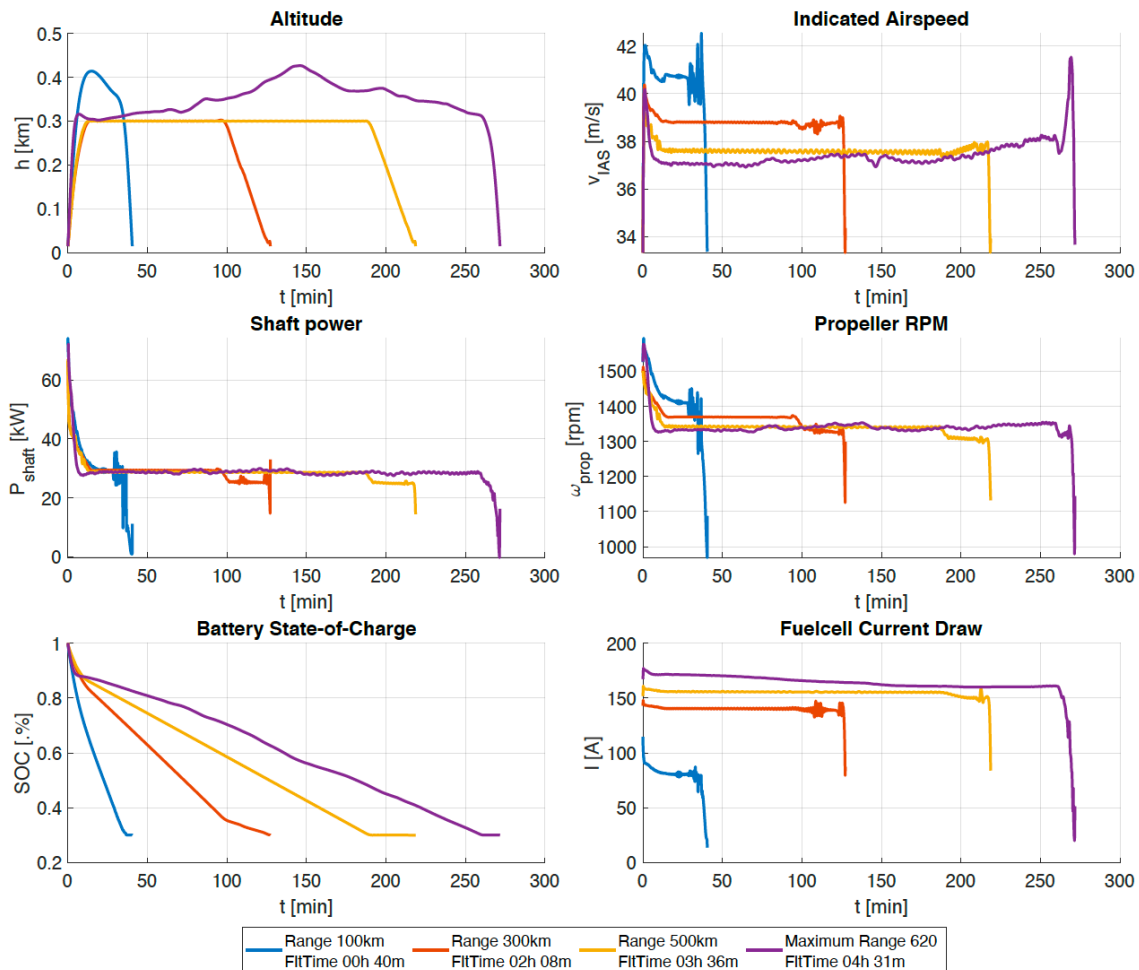
Fig. 17: Optimal flight trajectories for minimum fuel consumption, FCH *Pipistrel HY4*

Minimum time results are instead reported in Fig. 18: Optimal flight trajectories for minimum flight time, FCH *Pipistrel HY4* where it easy to note that, similarly to the case of the Panthera Electric Generator, the Fuel Cells are used at their maximum rate; on the other side, the flight trajectories heavily depend on the input range due to deficit of power and, the battery is discharge accordingly to the flown altitude and the airspeed.

17
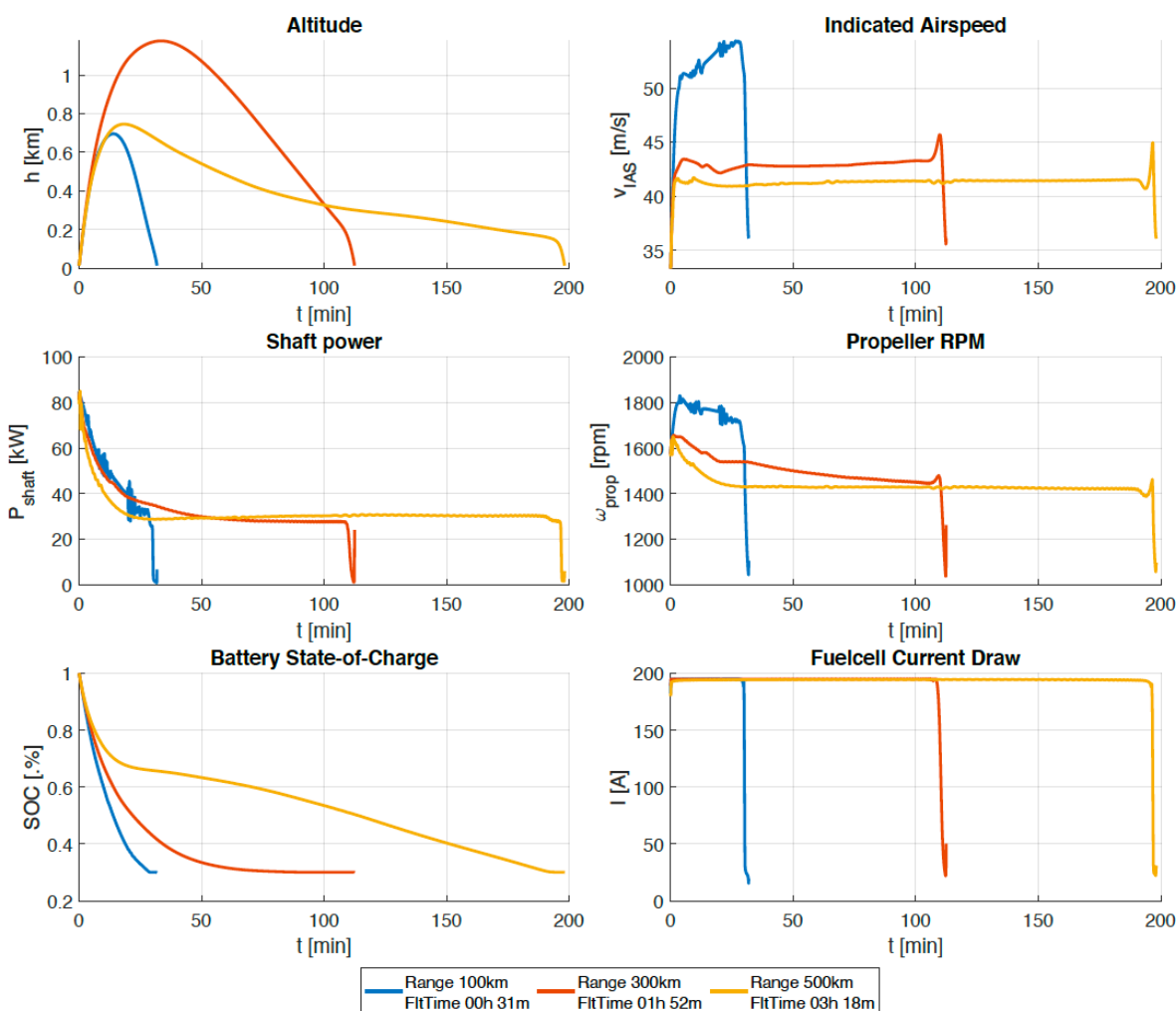
Fig. 18: Optimal flight trajectories for minimum flight time, FCH *Pipistrel HY4*

When comparing the global results as reported in Table 2, the benefits in terms of both flight time and fuel consumption are higher for shorter ranges, where more battery power is available. For shorter ranges, the fuel consumption in particular can be reduced by almost half when switching from a minimum time trajectory to a trajectory for minimum fuel consumption. On the other side, the difference in flight time is lower than in the case of the Panthera, mainly due again to the low available power. It is explicitly mentioned that the absolute weight save is negligible as the Hydrogen stored on board is very limited (14 kg).

Table 2: Comparison of global results for minimum time and minimum fuel, *FCH Pipistrel HY4*

| Range | Flight time Min. | Comparison with fuel-optimal case | | | |
		ΔFlight time [h:mm]	ΔFlight time [%]	Δ Fuel burn [kg]	Δ% Fuel burn [%]
100	0:31	-0:09	-22.5%	+0.9	+90.0%
300	1:52	-0:16	-12.5%	+1.2	+21.4%
500	3:18	-0:18	-8.3%	+1.4	+13.8%

18

In conclusion, a comparison of the power management strategies between HE and FCH aircraft is reported in Fig. 19, where the graphs are related to the case of an input range R=500 km and minimum fuel optimization. In this case, similar control strategy is observed, consisting in using the battery only to increase flight performance during climb. On the other side battery utilization is kept as low as possible during cruise in order to maximize the electric efficiency of the battery.
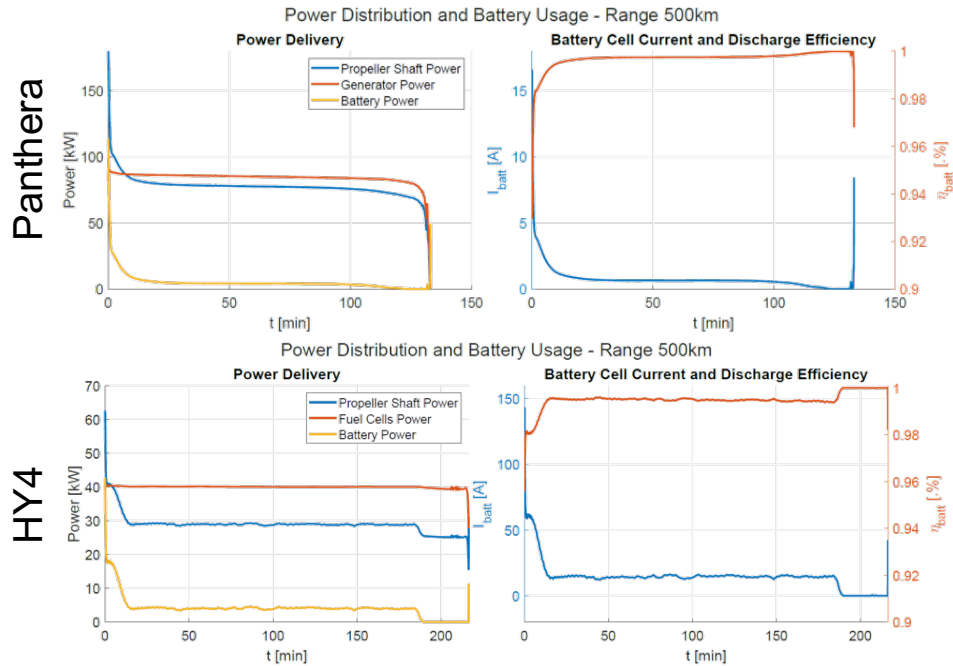
Fig. 19: comparison of power management, minimum fuel consumption, R=500 km

D. Results – Comparison of Multi-Phase and Single-Phase problems

The Multi-Phase problem is similar to a multi-segment problem, with the difference that each segment, now called a phase, is its own individual problem. This means each Phase can have different variable bounds, error tolerances, dynamics equations, cost functions. The Phases are linked together by the boundary link constraints, which ensure that the states, inputs, and time in the first point of a phase equal those in the last point of the previous phase. Five flight phases are defined. The first one, starting after the lift-off point, prescribes an obstacle-clearance climb. The first phase ends when an altitude of 150m is reached, and has the final distance as a boundary cost, resulting in a minimum distance climb. The next phase is a relatively free climb to an altitude of at least 300m. The only constraint added is the climb rate must be at least 0.1m/s. The cruise phase is constraint to a constant altitude, and is followed by a descent, again with a minimum descent rate of -0.1m/s. The descent phase transitions into a final descent phase at an altitude of 30m and at reference airspeed 1.3 times the stall speed.

Solution of a Multi-Phase problem is then plotted with respect the correspondent Single-Phase approach, in Fig. 20, when considering the minimum fuel problem for the Pipistrel Panthera, having an input range R=500 km. Fig. 20 shows that differences in the solution is negligible when looking at a global indicators such as the total burnt fuel or the total flight time. Controls in the Multi-Phase problem present small numerical oscillation, especially close to the phase linkage points, probably due to a rapid change of the constraints in the system dynamics. Biggest differences can be appreciated in the case of smaller range, but always leading to suboptimal results when compared to the Single-Phase approach.

19
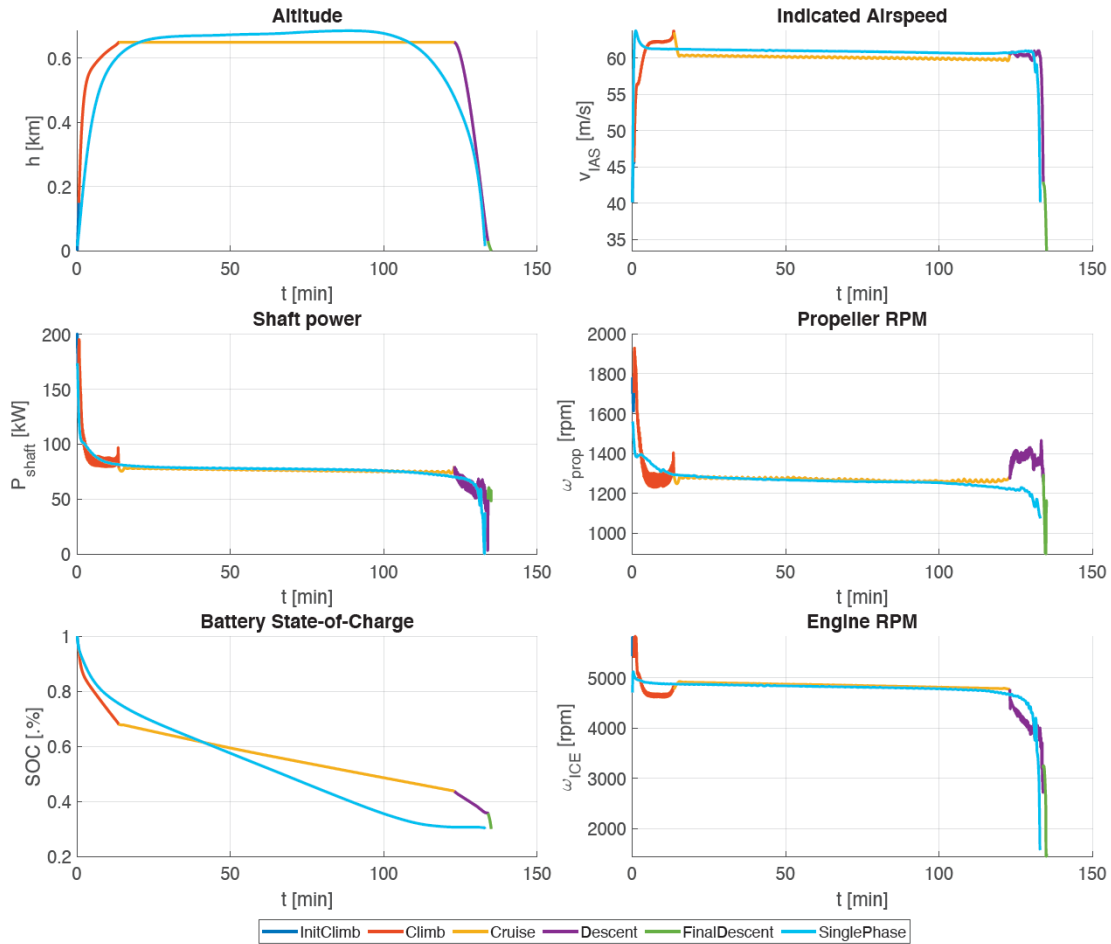
Fig. 20: Comparison between the single and multiphase solution for the HE Pipistrel Panthera R=500km

E. Results – Comparison of the resolution algorithms

The last analysis aims at evaluating the performance of the two resolution algorithms described in Section III (i.e. the *HS Direct Collocation* and the *LGR Pseudospectral*) when applied to the same Optimal Control Problem. The results are visualized in Fig. 21 for the HE Pipistrel Panthera, Minimum Time, Single-Phase. Both the algorithms converge to the same solution, both in terms of global indicators (total flight time) and time evolution of the controls and states. Therefore, the problems is considered to be robust enough and well posed.

Finally, the overall computational effort is reported in Table 3, for all the different Single-Phase optimization runs. It can be noted that for the more regular study cases (i.e. minimum time, HE Panthera), the LGR algorithm always outperforms the HS direct collocation, as expected. On the other side, when the solution is no longer regular and the numerical analysis has difficulties due to more demanding system dynamics, the LGR hardly converges to the optimum solution and oscillations in the states and controls start to occur. In the specific case, the HS algorithm is superior when applied to the FCH Pipistrel HY4 study case.
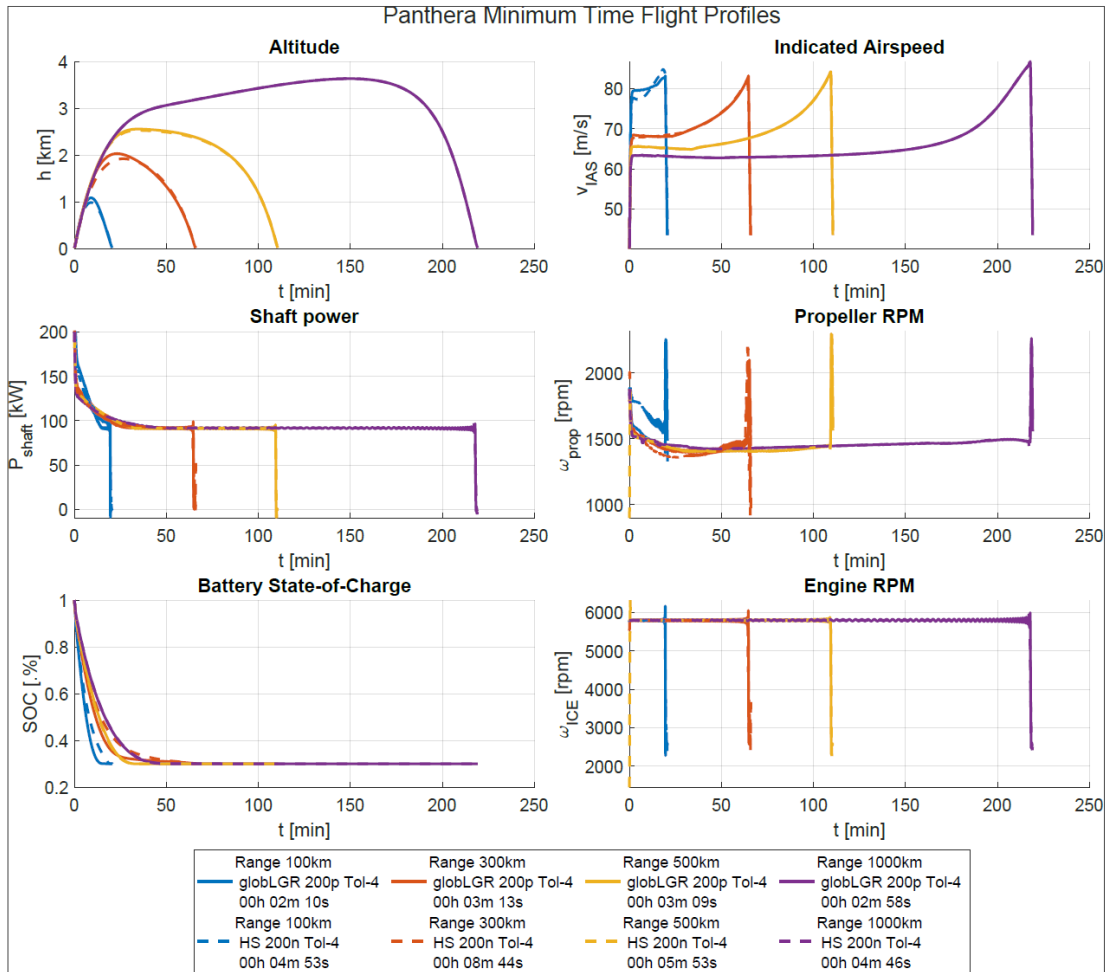
Fig. 21: Comparison of HS and LGR, HE Pipistrel Panthera, Minimum Time

Table 3: Computational time for different runs and algorithms (INTEL I7-1185G7 processor, 16 GB RAM)

	Range/ Algorithm	100km	300km	500km	1000km
Panthera (Single Phase)	**HS**	5min	9min	6min	5min
	LGR	2min	3min	3min	3min
HY4 (Single Phase)	**HS**	13min	1h	22min	-
	LGR	14min	3h23min	1h	-

IV. Conclusions

The present study demonstrates the capability of a tool properly developed in order to compute optimal mission parameters for the case of a generic Hybrid Aircraft. From a mathematical point of view, it consists of an Optimal Control problem where the overall system dynamics involve aircraft motion and powertrain simulation.

Two approaches are adopted: the first one, Single-Phase, has a less computational time and allow to determine a unique time-dependent evolution of the mission. The second one, Multi-Phase, has the possibility to model different flight segment at expenses of a heavier computational effort. In addition, two different algorithms have been tested on a variety of study cases and objective functions.

In principle, the tool is proven to be configuration agnostic: more specifically, the subroutines dedicated to the powertrain modelling, allow to describe multiple architecture and a variety of components following the modular approach developed in the early stages of the *Mahepa* Project. In addition, the tool allows to include a generic powertrain component by means of either experimental data sets or analytical relations that, have been used to model batteries and Fuel Cell operating characteristics.

The possibility to compare the simulator with data coming from a real flight test, gave the possibility to validate the effectiveness and the reliability of the used models for both the powertrain and the aircraft dynamics.

Several analyses have been run on two distinct aircraft configurations considering different objective functions related to minimization of the fuel or of the flight time. Results show that the overall energy management strategy for best fuel economy is similar for both the aircraft, even though both have different powertrain configurations and aerodynamic characteristics. The power source which consumes fuel, be it a fuel cell or a combustion engine, is run at an approximately constant power output corresponding to most of the power required during main or cruise section of the flight. Additional power required during take-off and climb is provided by the batteries. When looking at the overall indicators, minimum fuel flight allows to save from 10% to 25% of the total embarked fuel when compared to minimum flight time.

Using the Single-Phase problem definition, it is possible to identify general control targets such as best airspeed and power settings for best fuel economy during cruise. In case of the Panthera, defining these values is easy, considering the trajectories are consistent for all ranges. For the HY4, it is possible to identify the best airspeed, but altitude should be kept as low as possible, due to the climb requiring a high power load and causes higher energy loss. In general, this latter study case demonstrated to be challenging as the reduced available power limits further the feasible design space.

Using a Multi-Phase problem setup can offer more control over the trajectory, but results in a suboptimal solution because of the added constraints and costs and the numerical convergence is generally more difficult to be achieved. However, the Multi-Phase strategy seems to be the only possible alternative when different power mode (e.g. energy recuperation, full electric, battery charging) could be selected during the flight so that discontinuities in some of the states could be possible.

On both the aircraft analyses, differences in total fuel consumption were small when compared to variation in some of the states such as altitude profile or operating condition of the E-Motor. This behavior might indicate a relatively 'flat' objective function. For best fuel economy, flying at a minimum drag airspeed, and keep a constant power setting, proved more important than the choice of altitude. This was more noticeable for the HY4, with its relatively low power available and good aerodynamic properties following from its glider-based airframe.

For complex problems with a "smooth" solution, such as the minimum fuel case for the Panthera, LGR collocation yields both better results with lower objective values and does so in a fraction of the time compared to HS collocation. The difference in solutions obtained between the two methods reduces when switching to a simpler problem, like time minimization. However, LGR collocation is still faster and less sensitive to initial guesses. If the problem is complex, and has a less obvious solution, such as the fuel-optimal trajectory optimization for the relatively under-powered HY4, it appears the LGR-transcribed problem becomes too complex and the opposite becomes true.

Acknowledgments

References

[1] MAHEPA Consortium, *Modular Approach for Hybrid-Electric Propulsion Architecture*, URL: https://mahepa.eu/.

[2] Shelby M. E., *Aircraft Perfomance, Theory and Practice*, Butterworth-Heinemann, 2000.

[3] Casarosa C., *Meccanica del Volo*, Pisa University Press, 2013

[4] Torenbeek E.,"Optimum cruise performance of subsonic transport aircraft", Delft University Press Tech Report, 1998.

[5] Robert F.D., Chin J. C. Et Al, "Trajectory Optimization of Electric Aircraft Subject to Subsystem Thermal Constraints", *18th Multidisciplinary Analysis and Optimization Conference, AIAA AVIATION*, Denver, 2019.

[6] Robert F.D., Chin J. C. Et Al, "Development of a Multi-Phase Mission Planning tool for NASA X-57 Maxwell'' *Multidisciplinary Analysis and Optimization Conference, AIAA Aviation*, Atlanta, 2018.

[7] Kelly M. P. , *Transcription Methods for Trajectory Optimization A beginners tutorial*, Cornell University, 2015.

[8] Betts J. T., "Survey of Numerical Methods for Trajectory Optimization" *Journal of Guidance, Control and dynamics ,* Izv. 2, št. 2, 1998.

[9] ICLOCS2, Imperial College London Optimal Control Software, Version 2.5, Yuanbo Nie, Omar Faqir and Eric Kerrigan, 2018, Imperial College; http://www.ee.ic.ac.uk/ICLOCS/ (accessed on 09/2021).

[10] Falugi, P., Kerrigan, E., and VanWyk, E., "Imperial college London optimal control software user guide (ICLOCS)," *Department of Electrical and Electronic Engineering, Imperial College London, London, England, UK, 2010.*

[11] Nie, Y., Faqir, O., and Kerrigan, E. C., "ICLOCS2: Try this Optimal Control Problem Solver Before you Try the Rest," *2018 UKACC 12th International Conference on Control (CONTROL), IEEE, 2018, pp. 336–336.*

[12] Kelly, M., çAn Introduction to Trajectory Optimization: How to Do Your Own Direct Collocation," *SIAM Rev.*, Vol. 59, No. 4, 2017, p. 849–904. doi: 10.1137/16M1062569

[13] Rendon, S. V., "Trajectory planning based on collocation methods for multiple aerial and ground autonomous vehicles," Ph.D. Thesis, Universidad de Sevilla - Escuela Tecnica Superior de Ingenieria, 2015.

[14] Topputo, F., Zhang, C., "Survey of Direct Transcription for Low-Thrust Space Trajectory Optimization with Application", Hindawi Publishing Corporation, Abstract and Applied Analysis, Volume 2014, doi: 10.1155/2014/851720.

[15] Pethersen, C., "Weather-Adaptive Noise Abatement Procedures Using Optimal Control", Master Thesis, Delft University of Technology, 2018.

[16] Barbir, F., *PEM fuel cells: theory and practice*, 2nd ed., Elsevier/Academic Press, 2013.

[17] Honwen H., Xiong R., Fan J., "Evaluation of Lithium-Ion Battery Equivalent Circuit Models for State of Charge Estimation by an Experimental Approach" *Energies, Izv. 4, pp. 582-598, 2011*.

[18] Piccio, M.E., Porrini, A. "Planning and simulation of the flight test campaign of a hydrogen hybrid-electric aircraft", Master Thesis, Politecnico di Milano, 2020.